(Received 16 August 2024, Accepted 8 October 2024, Scheduled 14 November 2024)

Grating Lobe Performance Improvement of an Arbitrarily Spaced Array of Through-the-Wall Imaging Radars Using Time Reversal Techniques

Paramananda Jena[1] and Kedar Nath Sahu[2, *]

[1] *Electronics and Radar Development Establishment (LRDE)*
Defence Research and Development Organisation (DRDO), Bengaluru, India
[2] *Department of Electronics and Communication Engineering*
Stanley College of Engineering and Technology for Women, Hyderabad, India

ABSTRACT: This paper presents a Time Reversal (TR) application to mitigate the grating lobes of an arbitrarily spaced array for a through-the-wall imaging radar (TWIR). Analytical modeling and simulation of array of arbitrarily located elements with (i) conventional and (ii) time reversal beamforming have been carried out. The results are analysed and compared. The array is used to image a target using the multipaths in a typical TWIR environment. The Time Reversal technique as spatial correlator improves the performance of the arbitrarily located array which is akin to the array thinning of conventional array processing. It is demonstrated that the TR beamforming can mitigate the grating lobes of large sparse array with a fewer elements. The performance metrics are captured in terms of Side Lobe Levels (SLLs) and image radius. The SLL performance and image radius are benchmarked for different configurations of array. It is shown that a fewer-element sparse array with Time Reversal is feasible for practical TWIRs.

1. INTRODUCTION

Ultra-wideband (UWB) radars [1, 2] with MIMO configurations are used for imaging applications such as Ground Penetrating Radar (GPR), Through-the-Wall-Imaging Radar (TWIR), and also urban sensing applications. The low frequency component of UWB waveform easily penetrates the barrier while the high frequency component aids in finer resolution. UWB TWIRs [3] are used by police and military forces for hostage rescue operation, rescue of earth quake victims, and fire-fighting personnel. The use of such radars is extended for other civilian applications like detection of human fall and human gait movement in a room [4]. Finer resolution both in down range and cross range is of paramount importance for target detection, tracking, and classification. The larger the bandwidth is, the finer the range resolution is. Due to the advent of wideband waveform, it is easy to generate high bandwidth waveform. The major issue is to obtain high cross range resolution, that is, in both azimuthal and elevational dimensions. The larger the size of the array is, the finer the resolution is [5]. The design of TWIR array antenna has been attempted with various techniques. In order to have high resolution, a UWB radar needs a large antenna array with real or synthetic aperture. The commonly used TWIR configurations are monostatic, bistatic/multistatic, and Multiple Input Multiple Output (MIMO). In recent years, MIMO radars [6, 7] have been used for TWIR application. Applications of UWB MIMO sparse array for both impulse and Stepped Frequency Continuous Wave (SFCW) types have been reported in [2]. The research attempts have been to use thinned, sparse and MIMO arrays to reduce the number of elements. Sparse array results in poor side lobe and grating lobe [5]. The objective of TWIR is to obtain clean image of targets in the presence of clutter. The primary cause of image artefacts is due to poor side lobe and grating lobe performance of an array. Usually, the side lobes are controlled by using either a standard window technique or modern optimisation scheme, namely genetic algorithms [8]. The grating lobe performance of an array is the direct function of the spacing between array elements, steering angle, and the bandwidth of the waveform [5]. The MIMO co-array technique [9] for UWB SFCW radar is one such technique, where superior grating lobe performance can be obtained through suitable placement of transmitting and receiving elements, but it is limited by the size of the co-array. The Time Reversal technique based virtual arrays are proposed for the passive direction finding [10]. Compressive sensing (CS) technique is usually used for the direction of arrival (DoA) estimation in sparse antenna array in L-shaped antenna [11, 12]. The wideband sparse array design is formulated using quadratically constraint quadratic program based on tapped delayline and DFT techniques. The semidefinite relaxation (SDR) is used to achieve the sparse array and to yield better performance than a sub-optimal sparse array [13]. Deep learning (DL) based sparse array antenna using hole-free co-arrays can improve the beam pattern and DoA [14]. The Time Reversal (TR) is an emerging signal processing technique, which promises superresolution in the multipath-rich environment. By the use of TR, the multipath reflections result in a

* Corresponding author: Kedar Nath Sahu (skedarnath@stanley.edu.in).

virtual array which provides better resolution. The virtual array size is a function of the distribution of multipaths. All the scatterers result in virtual transmitters and receivers. So after the application of TR, as the virtual array randomisation of the elements happens, there will not be any periodicity in the array pattern, and hence the grating lobes get reduced.

The multipath reflections from scatterers like walls, floors, and ceiling are treated as nuisance for conventional TWIR processing. High resolution waveform and frequency diversity, popularly used by the radar community [15] to suppress or mitigate the multipath effects, are directly used in TWIR. There is entirely an opposite view to develop a technique which exploits the presence of the multipaths, that is, the more the multipaths are, the better the performance is. In the opinion of the authors, two distinct classes of multipath exploitation techniques are used in TWIR. One technique is based on the known geometry of the room [16, 17] from which the ghost target can be mapped back to the original target position to improve the signal to clutter ratio (SCR). The other technique is the one that is TR based and does not assume the geometry of the building. The Time Reversal (TR) concept [18–22] uses the time invariant properties of wave equation. It was initially used in acoustics and is now becoming popular in electromagnetics as well. In the case of non-homogeneous multipath environment, TR promises super-resolution better than the Rayleigh resolution limit [20, 23]. The transmitting and receiving array lengths of a TWIR are based on the resolution requirement. The smaller the antenna size is, the poorer the angular resolution is, but the larger array increases the weight of the radar. Under such circumstance, a sparse array is the best solution, as it provides better resolution due to large size and moreover, less weight due to a few elements in the array. The major concern is due to the grating lobe of a sparse array, as it results in ghost targets and poorer imaging quality. The image of a typical TWIR target, e.g., human being, merges in multipath reflections from scatterers like household furniture such as tables, cupboards, chairs, walls, floors, and ceiling. Ghost targets are also generated due to a large number of multipaths. Time Reversal (TR) technique exploits multipaths to provide an improved resolution. The grating lobe performance using TR has been studied analytically [24]. To the best of our knowledge, the development of TR based grating lobe suppression for an arbitrarily spaced array of UWB radar is a novel technique.

In this paper, a real aperture MIMO SFCW radar with arbitrary location of receivers and transmitters is used to study the effect of TR on grating lobe processing. The proposed TR based signal processing scheme is used in a sparse MIMO array in a TWIR like propagation through the wall and scattering of multiple objects and wall. The grating lobes are suppressed and quantified both in the presence and absence of the multipaths. It is an important finding that can potentially reduce the weight and size of TWIR without compromising its performance. To validate the grating lobe performance of TR technique for TWIR, multiple scatterers and targets have been modeled using analytical electromagnetic equations in order to mimic a through-the-wall (TTW) imaging scenario. The organisation of the paper is as follows.

Section 2 introduces the features of antenna arrays for TWIR imaging, particularly consisting of widely separated antennas. The Time Reversal focusing with array antenna is detailed in Section 3. Section 4 presents the MATLAB simulation results. The conclusion of the work is given in Section 5.

2. WIDELY SEPARATED ANTENNA ARRAY FOR IMAGING

The uniform linear array (ULA), spatial sampling, and theory of gating are presented here. Widely spaced antenna array where the element spacing is more than one wavelength λ generates grating lobes [5]. The array samples the electromagnetic fields spatially at the locations denoted as $r_i;\ i = 0, 1, 2, \ldots N-1$. The received signal at the arbitrarily located array can be given by Equation (1).

$$s(t,r) = [s(t,r_0), s(t,r_1), s(t,r_3) \ldots, s(t,r_{N-1})]^T \quad (1)$$

With reference to the nonuniform linear array (non-ULA) shown in Figure 1, the relationship between direction cosines and angle of arrival can be expressed as,

$$u = \sin\theta, \quad (2)$$

where u represents the direction cosines with respect to the array axis, and θ is the angle of arrival with respect to the array normal.

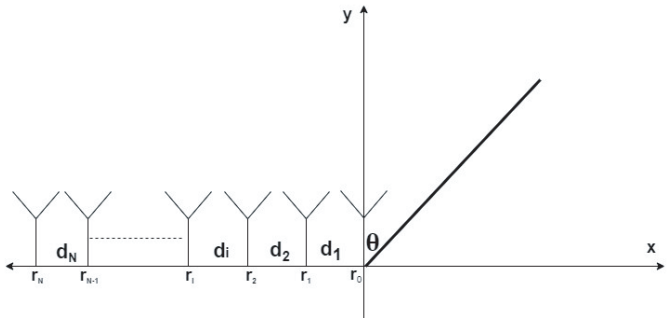

FIGURE 1. Non-uniform linear array.

The beam pattern $B(\omega, \theta)$ of the above nonuniform linear array at frequency ω and angle θ can be given by,

$$B(\omega,\theta) = \sum_{n=0}^{N-1} \omega\, e^{-jnkd_n \sin\theta}, \quad (3)$$

where d_n is the inter element distance, and N is the number of elements in the array.

2.1. Theory of Array Synthesis and Grating Lobe

Considering a uniform linear array (ULA) of element spacing, d, and direction of arrival, θ, as shown in Figure 2, its array factor as reported in [5] is given by Equation (4).

$$B_\psi(\psi) = \frac{\sin\frac{N\psi}{2}}{N\sin\frac{\psi}{2}}, \quad (4)$$

$$\text{where,} \quad \psi = \frac{2\pi}{\lambda} d\sin\theta. \quad (5)$$

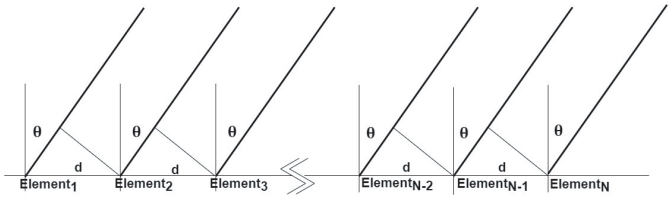

FIGURE 2. Uniform linear array.

The grating lobe is of the same height as the main lobe. It appears corresponding to θ.

$$\frac{\psi}{2} = m\pi \tag{6}$$

From Equations (2), (5), and (6), we get,

$$u = \frac{m\lambda}{d} \tag{7}$$

If wavelength $\lambda > d$, then, the peak of the grating lobe occurs within the propagation space of the signal, that is, when $|u| \leq 1$. In the case of steering, the grating lobe gets shifted into the visible region. If the array is required to be steered over the range, $0 \leq \theta \leq 180°$, the required spacing is $d \leq \frac{\lambda}{2}$. The grating lobe problem is similar to the aliasing problem of the time series.

2.2. Beam Pattern of SFCW Waveform

In the case of an SFCW waveform, the grating lobe of each step gets averaged out in the UWB beamforming operation. The patterns of the start, center, and end frequencies are shown in Figure 3 in order to explain the grating lobe effect of SFCW waveform. SFCW mitigates the side lobes naturally; however, for arbitrarily spaced elements, the side lobe performance is not very useful for practical sparse array based TWIR.

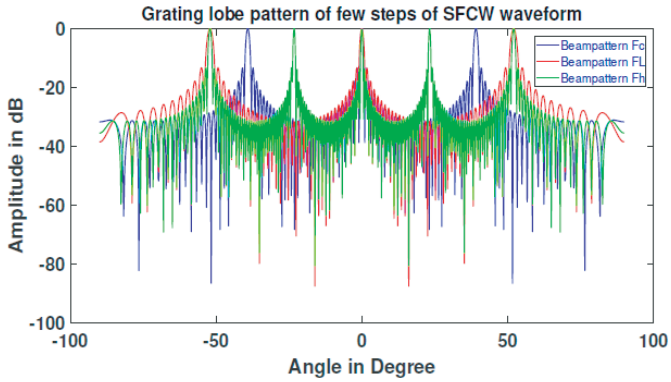

FIGURE 3. Beam pattern for spot frequency of SFCW waveform.

The beam pattern of SFCW waveform due to the interference of the grating lobes corresponding to each individual frequency reduces the amplitude of the array grating lobes. The resultant grating lobe of SFCW beam is depicted in Figure 4.

Further, the suppression of grating lobes using TR technique is described in Section 3.

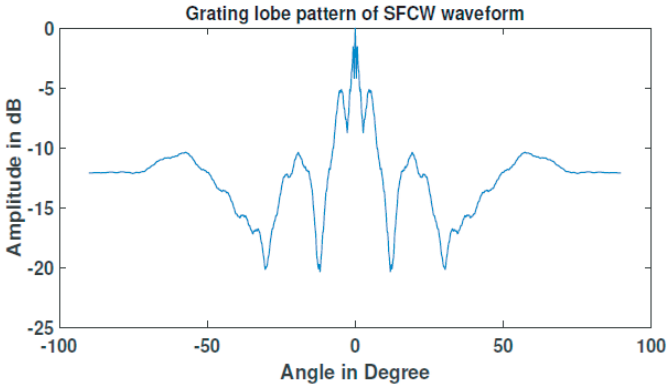

FIGURE 4. Beam pattern of SFCW UWB beamforming.

3. TIME REVERSAL FOCUSING WITH ARRAY ANTENNA

In Figure 5, r_o (x_o, y_o) represents the point source or target locations. The receiving array r_i (x_i, y_i) receives the signal from the point source (active) or reflections from the passive target. The time-reversal array (TRA) receives the signals and then transmits. r_q (x_q, y_q) denotes the arbitrary locations in image domain.

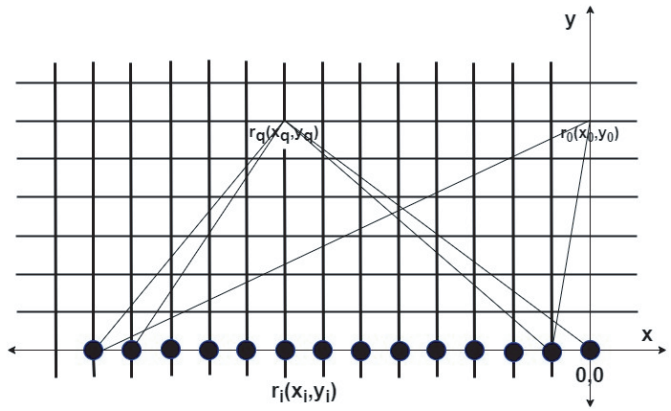

FIGURE 5. Imaging with time reversal array.

Let $s_T(t)$ be the transmit signal and $S_T(\omega)$ be its spectrum. Then, it can be written that,

$$s_T(t) = \frac{1}{2\pi}\int S_T(\omega)e^{j\omega t}d\omega, \tag{8}$$

$$\text{and} \quad S_T(\omega) = \int s_T(t)e^{-j\omega t}dt \tag{9}$$

Now, the received signal spectrum can be expressed as,

$$S_R(\omega) = \int G_i(r_i, r_0, \omega)S_T(\omega), \tag{10}$$

where $G_i(r_i, r_0, \omega)$ is the Green's function between r_0 and r_i.

For r_i locations, Equation (10) can be written as,

$$S_R(r_i, \omega) = \int G_i(r_i, r_0, \omega)S_T(\omega) \tag{11}$$

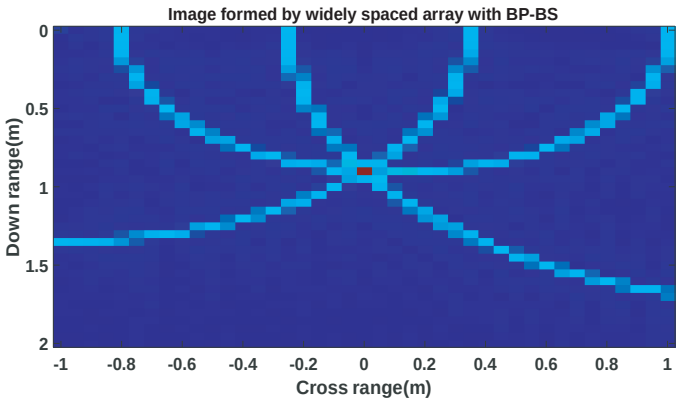

FIGURE 6. Grating lobe with BP-BS (three-element array).

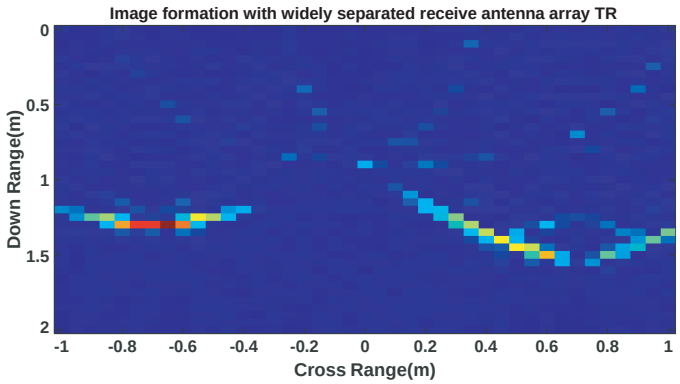

FIGURE 7. Grating lobe with BP-TR (three-element array).

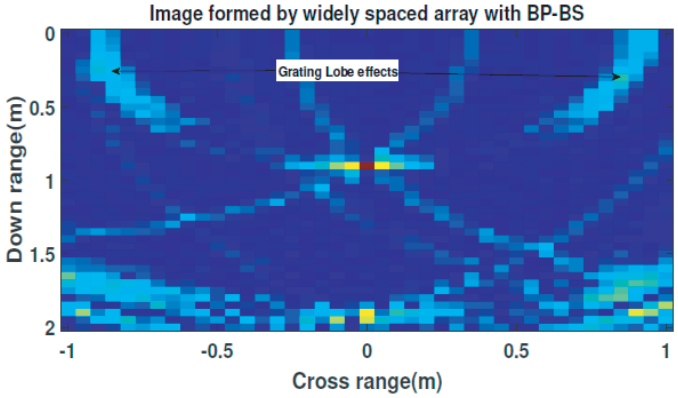

FIGURE 8. Grating/side lobe with BP-BS (five-element array).

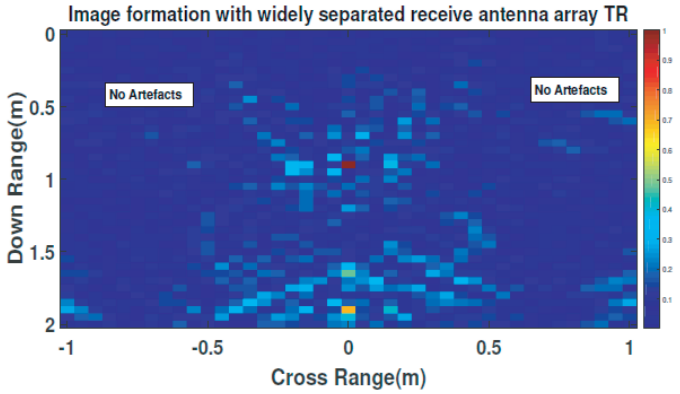

FIGURE 9. Grating lobe with BP-TR (five-element array).

Then, in time domain,

$$s_R(r_i, -t) = \frac{1}{2\pi} \int G_i^*(r_i, r_0, \omega)\, S_T^*(\omega) \tag{12}$$

$s_R(r_i, -t)$ is the time reversal of $s_r(r_i, t)$ and is denoted as $s_{TR}(r_i, t)$. Thus,

$$s_{TR}(r_i, t) = s_r\,(r_i, -t) \tag{13}$$

In frequency domain,

$$s_{TR}(r_i, \omega) = G_i^*(r_i, r_0, \omega) S_T^*(\omega) \tag{14}$$

The time reversed pulse observed at the location r_q is given by,

$$s_{TR}(r_q, r_i, t) = \frac{1}{2\pi} \int G_i(r_q, r_i, \omega) G_i^*(r_i, r_0, \omega) S_T^*(\omega) e^{j\omega t} d\omega \tag{15}$$

The general formula for the time reversal of an array can be given by,

$$s_{TR}(r_q, t) = \sum s_{TR}(r_q, r_i, t) \tag{16}$$

Using $g_q = [G_{q0}, G_{q2}, \ldots G_{q(N-1)}]$ and $g_0 = [G_0, G_2, \ldots G_{N-1}]^T$, we can have,

$$s_{TR}(r_s, t) = \sum_{i=0}^{N-1} \frac{1}{2\pi} \int g_q^T g_0^* S(\omega) e^{-j\omega t} dt \tag{17}$$

Here, g_q and g_0 are the Green's functions using the matrix representations.

The above analysis is then implemented in MATLAB.

4. SIMULATION RESULTS AND DISCUSSION

The simulation setup is established for one target and a few scatterers assuming that the scatterers are close to the wall. The closeness of the scatterers to the target and the superresolution performance of TR array are studied. The details of the parameters used for the simulation are presented in Table 1. The simulation results corresponding to the widely spaced receive antenna arrays for grating lobes with back projection (BP) of different profiles like BS and TR are obtained and plotted as shown in Figure 6 through Figure 13. The variations of the amplitude gain with the distance from the active source are obtained from the simulations of the cross-range profiles for the

TABLE 1. Distributed array simulation parameters.

parameters	value	parameters	value
Room size	2 m × 2 m	Δf	10 MHz
Length of array	2.5 m	Range (unambiguous)	15 m
No. of Tx	1	Target	0.9 m
No. of Rx	3, 5, 7	BW	2–4 GHz

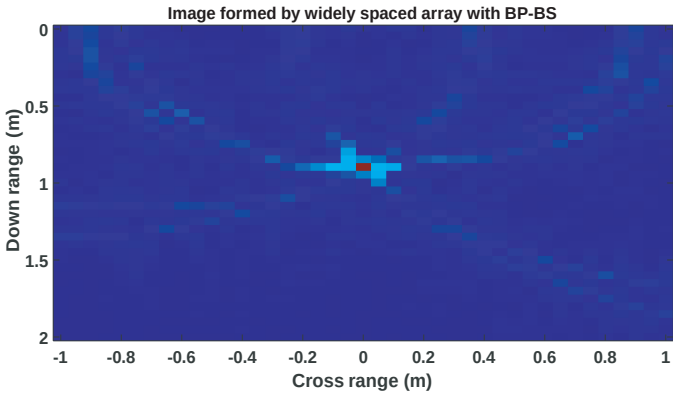

FIGURE 10. Grating/side lobe with BP-BS (seven-element array).

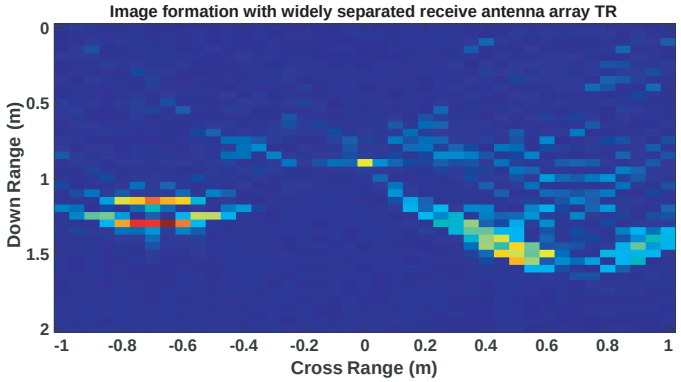

FIGURE 11. Grating/side lobe with BP-TR (seven-element array).

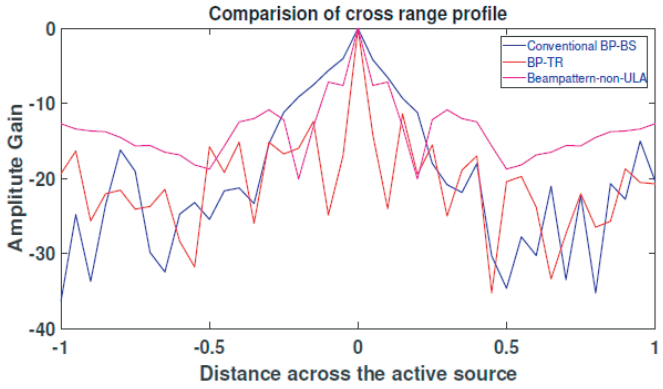

FIGURE 12. Comparison of cross range profiles for conventional BP-BS, BP-TR and beam pattern (non-ULA).

FIGURE 13. Cross-range profiles, BP and TR applied to a non-ULA.

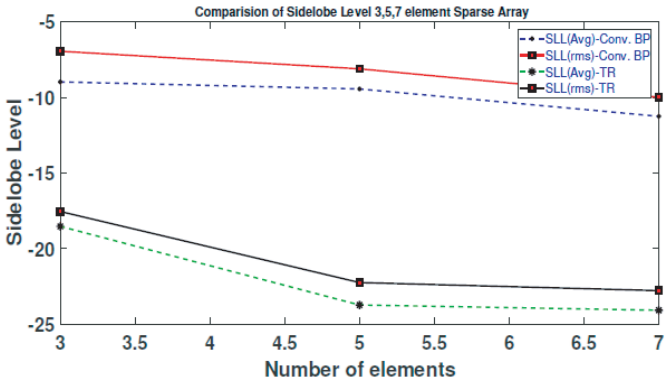

FIGURE 14. Improvement of side-lobe level for 3, 5, and 7 element non-ULA.

(i) conventional back projection-back scatter (BP-BS), (ii) back projection-time reversal (BP-TR), and (iii) beampattern (non-ULA) as shown in Figure 14. Finally, the variations of the image intensity with the cross range are obtained from the simulations of the cross-range profiles; BP and TR for (i) 3-, (ii) 5-, and (iii) 7-element sparse array and the superimposed results are shown in Figure 13 and Figure 14.

The summary of comparison (Figure 12) is shown in Table 2.

TABLE 2. Cross-range resolution and SLL of non-ULA TWIR (five-element).

Parameters	BP-BS	TR-correlator	Beam pattern
Cross range resolution	0.1 m	0.018 m	0.075 m
SLL at 0.3 m from the center	−10 dB	−14 dB	−10 dB
SLL at 0.5 m from the center	−13.84 dB	−14.4 dB	−13 dB

4.1. Discussion

The typical imaging of non-ULA with five elements is shown in Figure 8. It is evident that the image artifacts due to the grating/side lobes are more. But with the application of TR, the grating/side lobe is minimized as depicted in Figure 9. The comparison of (a) theoretical beam pattern of UWB non-ULA, (b) imaging by back-projection, and (c) TR spatial focusing has been performed. It is observed that the TR not only provides superresolution, but also suppresses the grating lobes or side lobes. Firstly, the nonuniform array with UWB SFCW waveform reduces the grating lobe. The random scattering media with TR reduces the grating lobe to an extent more than the

interfering pattern of the grating lobes pertaining to each frequency step of the SFCW waveform. The parameterization for the comparison of grating/side lobes is described in Section 4.1.1.

4.1.1. Side Lobe Level (SLL)

The poor side lobes both in down range and cross range dimensions create unnecessary image artifacts in the radar based imaging systems. There are two performance metrics, namely, average side lobe level (SLL_{avg}) and RMS side lobe level (SLL_{rms}) used to validate the performance improvement in a widely spaced TWIR array using TR processing. In order to study the grating lobe performance for a widely separated array, the polar plot, that is, the (r, θ) domain is introduced for the analysis.

(i) **Average Side Lobe Level (SLL_{avg}):** The average value of the side lobes excluding the main lobe targets is given by Equation (18).

$$SLL_{avg} = \frac{1}{N_\theta} \sum_{n=1}^{N_\theta} I\left(r_t, \theta_n\right), \tag{18}$$

where N_θ is the number of discrete azimuth angles from $-\pi/2$ to $\pi/2$, and $I(r_t, \theta_n)$ denotes the intensity of the image pixels at the target locations.

(ii) **RMS Side Lobe Level (SLL_{rms}):** The rms value of the side lobes excluding the main lobe targets is given by Equation (19).

$$SLL_{rms} = \sqrt{\frac{1}{N_\theta} \sum_{n=1}^{N_\theta} I^2\left(r_t, \theta_n\right)} \tag{19}$$

The improvement in side and grating lobe performances of three TWIR array configurations of arbitrary locations such as TWIR array with (i) 3, (ii) 5, and (iii) 7 receiving elements are studied. The results are shown in Figure 14 and Table 3.

TABLE 3. SLL of non-ULA TWIR.

SLL (dB)	Back projection (dB)	TR-Correlator (dB)
Three-element array		
SLL Avg.	-8.98	-18.52
SLL rms	-6.95	-17.54
Five-element array		
SLL Avg.	-9.44	-23.71
SLL rms	-8.11	-22.23
Seven-element array		
SLL Avg.	-11.25	-24.06
SLL rms	-9.99	-22.7

The side and grating lobe level degradation in arbitrarily placed arrays is captured in terms of the average side lobe level difference with respect to the conventional back projection imaging.

There is improvement of 10, 14, and 13 dB in the 3-, 5-, and 7-element arrays, respectively. This improvement is significant for imaging applications and thus confirms the robustness of Time Reversal against the degradation image due to the grating lobes in a sparse array.

4.1.2. Image Radius

The smearing effect of the images obtained by applying back-projection and TR-correlator is captured through the measurement of image radius. The image radii are estimated with a normalized threshold of 0.2 and 10×10 pixel around the target image. The image radii of the same three TWIR array configurations considered as above with (i) 3, (ii) 5, and (iii) 7 receiving elements are obtained. The results are shown in Table 4. It is observed that the imaging radius with smaller value yields more focused image in the case of arrays of more elements.

TABLE 4. Image radius of the image formed using non-ULA TWIR.

Image radius	Back projection-image radius (cm)	TR Correlator-image radius (cm)
Three-element array		
Image Radius	20	14
Five-element array		
Image Radius	20	13
Seven-element array		
Image Radius	18	6

5. CONCLUSION

In this work, the Time Reversal technique is applied to a non-uniformly spaced antenna array of a TWIR radar. The image degradation due to the grating lobes of an arbitrarily spaced array with conventional beamformer has been compared with that of a Time Reversal correlator based beamformer. It is evident that the proposed Time Reversal correlator improves the grating lobe performance of an arbitrarily located UWB TWIR radar. The fewer array elements and arbitrarily spaced TR array for TWIR are advantageous at solving the problem of cross resolution and providing better portability. These features are substantiated from analytical methods as well as MATLAB simulations using the metrics such as SLL and image radius of arrays of different lengths.

REFERENCES

[1] Taylor, J. D., *Ultra-wideband Radar Technology*, CRC press, 2000.

[2] Yarovoy, A. G. and L. P. Ligthart, "Uwb radars: Recent technological advances and applications," in *2007 IEEE Radar Conference*, 43–48, Waltham, MA, USA, 2007.

[3] Amin, M. G., *Through-the-Wall Radar Imaging*, CRC Press, 2017.

[4] Amin, M. G., *Radar for Indoor Monitoring: Detection, Classification, and Assessment*, CRC Press, 2017.

[5] Van Trees, H. L., *Optimum Array Processing: Part IV of Detection, Estimation, and Modulation Theory*, John Wiley & Sons, 2002.

[6] Bliss, D. W. and K. W. Forsythe, "Multiple-input multiple-output (MIMO) radar and imaging: Degrees of freedom and resolution," in *The Thrity-Seventh Asilomar Conference on Signals, Systems & Computers, 2003*, Vol. 1, 54–59, Pacific Grove, CA, USA, 2003.

[7] Fishler, E., A. Haimovich, R. Blum, D. Chizhik, L. Cimini, and R. Valenzuela, "MIMO radar: An idea whose time has come," in *Proceedings of the 2004 IEEE Radar Conference (IEEE Cat. No.04CH37509)*, 71–78, Philadelphia, PA, USA, 2004.

[8] Cao, H., T. Jiang, and X. Chen, "Array optimization for MIMO radar by particle swarm algorithm," in *Proceedings of 2011 IEEE CIE International Conference on Radar*, Vol. 1, 99–103, Chengdu, Sichuan, China, 2011.

[9] Li, Z., T. Jin, B. Chen, and Z. Zhou, "A coarray based MIMO array design method for UWB imaging," in *IET International Conference on Radar Systems (Radar 2012)*, Glasgow, UK, 2012.

[10] Fu, Y. and Z. Yu, "A low SNR and fast passive location algorithm based on virtual time reversal," *IEEE Access*, Vol. 9, 29 303–29 311, 2021.

[11] Mirza, H. A., M. A. Z. Raja, N. I. Chaudhary, I. M. Qureshi, and A. N. Malik, "A robust multi sample compressive sensing technique for DOA estimation using sparse antenna array," *IEEE Access*, Vol. 8, 140 848–140 861, 2020.

[12] Hamza, S. A. and M. G. Amin, "Sparse array beamforming design for wideband signal models," *IEEE Transactions on Aerospace and Electronic Systems*, Vol. 57, No. 2, 1211–1226, 2021.

[13] Rajamäki, R., S. P. Chepuri, and V. Koivunen, "Hybrid beamforming for active sensing using sparse arrays," *IEEE Transactions on Signal Processing*, Vol. 68, 6402–6417, 2020.

[14] Wandale, S. and K. Ichige, "Design of sparse arrays via deep learning for enhanced DOA estimation," *EURASIP Journal on Advances in Signal Processing*, Vol. 2021, No. 1, 17, 2021.

[15] Skolnik, M. I., *Introduction to Radar Systems*, Mcgraw-Hill, New York, 1980.

[16] Setlur, P., G. Alli, and L. Nuzzo, "Multipath exploitation in through-wall radar imaging via point spread functions," *IEEE Transactions on Image Processing*, Vol. 22, No. 12, 4571–4586, 2013.

[17] Setlur, P., M. Amin, and F. Ahmad, "Multipath model and exploitation in through-the-wall and urban radar sensing," *IEEE Transactions on Geoscience and Remote Sensing*, Vol. 49, No. 10, 4021–4034, 2011.

[18] Jin, Y., J. M. F. Moura, N. O'donoughue, M. T. Mulford, and A. A. Samuel, "Time reversal synthetic aperture radar imaging in multipath," in *2007 Conference Record of the Forty-First Asilomar Conference on Signals, Systems and Computers*, 1812–1816, Pacific Grove, CA, USA, 2007.

[19] Jin, Y. and J. M. Moura, "TR-SAR: Time reversal target focusing in spotlight sar," in *2007 IEEE International Conference on Acoustics, Speech and Signal Processing — ICASSP '07*, 957–960, Honolulu, HI, USA, 2007.

[20] Lerosey, G., J. d. Rosny, A. Tourin, A. Derode, G. Montaldo, and M. Fink, "Time reversal of electromagnetic waves," *Physical Review Letters*, Vol. 92, No. 19, 193904, 2004.

[21] Moura, J. M. F., Y. Jin, D. Stancil, J.-G. Zhu, A. Cepni, Y. Jiang, and B. Henty, "Array processing using time reversal: Experiments and performance," in *2006 IEEE International Conference on Acoustics Speech and Signal Processing Proceedings*, Vol. 4, IV–IV, Toulouse, France, 2006.

[22] Yavuz, M. E. and F. L. Teixeira, "Ultrawideband microwave sensing and imaging using time-reversal techniques: A review," *Remote Sensing*, Vol. 1, No. 3, 466–495, 2009.

[23] Fink, M., D. Cassereau, A. Derode, C. Prada, P. Roux, M. Tanter, J.-L. Thomas, and F. Wu, "Time-reversed acoustics," *Reports on Progress in Physics*, Vol. 63, No. 12, 1933, 2000.

[24] Shi, G. and A. Nehorai, "Maximum likelihood estimation of point scatterers for computational time-reversal imaging," *Commun. Inf. Syst.*, Vol. 5, No. 2, 227–256, 2005.